Contrib Mineral Petrol (2002) 143: 673–683
DOI 10.1007/s00410-002-0368-3

Ilya V. Veksler · Rainer Thomas

An experimental study of B-, P- and F-rich synthetic granite pegmatite at 0.1 and 0.2 GPa

Received: 28 February 2002 / Accepted: 12 April 2002 / Published online: 23 May 2002

Abstract Extreme enrichment in H_2O, B, P and F is characteristic of many evolved granites and pegmatites. We report experimental phase relations of a synthetic peraluminous pegmatite spiked with P_2O_5, B_2O_3 and F (5 wt% of each), Rb_2O, Cs_2O (1 wt% of each) and Li_2O (0.5 wt%). Experiments were carried out in H_2O-saturated conditions in cold-seal rapid-quench pressure vessels at 0.1–0.2 GPa. Crystallisation starts at about 820 °C with berlinite and topaz. Quartz appears at 700–750 °C. Topaz is replaced by muscovite at about 600 °C. At near-solidus temperatures (450–500 °C) amblygonite, lacroixite and a Cs-bearing aluminosilicate crystallise. In all charges aluminosilicate melt coexists with low-density hydrous fluid and hydrosaline melt. The latter is strongly enriched in Na_3AlF_6 and H_3BO_3 components. Experimental evidence of the liquid immiscibility and mineral reactions documented in our study offers new explanations of many enigmatic features of natural pegmatites.

Introduction

Granitic pegmatites are exotic and enigmatic igneous rocks. Huge crystals, large monomineralic zones, unusual textures, extensive chemical and mineralogical zonation, extreme element enrichment and genetic links to rare-element ores, signs of fluid exsolution and mineral replacement – these and other puzzling features have not had a satisfactory explanation from existing theories of pegmatite formation.

I.V. Veksler (✉) · R. Thomas
GeoForschungsZentrum Potsdam,
Telegrafenberg, 14473 Potsdam, Germany
E-mail: veksler@gfz-potsdam.de
Tel.: +49-331-2881425
Fax: +49-331-2881474

Editorial responsibility: J. Hoefs

Classical models of pegmatite formation (e.g. Jahns and Burnham 1969) emphasise the importance of fluid-melt phase separation early in pegmatite evolution, and state that volatile-saturated aluminosilicate melt and coexisting, low-density aqueous fluid determine pegmatite evolution. These views have been challenged by a number of experimental studies showing that supercritical behaviour in pegmatitic systems is possible (London 1986; Sowerby and Keppler 2002), and models have been proposed which relate typical zonation of pegmatite bodies to crystallisation and zone refinement of a single supercooled liquid (London 1992, 1999). On the other hand, phase equilibria studies in some crucial salt-water systems, such as H_2O–NaCl (Sourirajan and Kennedy 1962; Bodnar et al. 1985), and numerous studies of natural melt and fluid inclusions in pegmatite minerals (Roedder 1992) imply that aluminosilicate melt may coexist in a stable form with not one but two hydrous fluids of contrasting salinity early in the course of pegmatite evolution (Shmulovich and Churakov 1998). Thus, there may be as few as one and as many as three coexisting fluids involved in the development of pegmatites.

Based on differences in the type of chemical bonds and affinities to the three potential pegmatitic fluids (silicate melt, hydrosaline melt, and dilute hydrous fluid), the chemical components of pegmatitic systems can be divided into three groups: (1) main constituents of aluminosilicate melts (SiO_2, Al_2O_3, FeO, K_2O, Na_2O, Li_2O and other, less abundant oxides); (2) borates, phosphates, fluorides and chlorides of alkaline and alkaline earth elements (here united under general term "fluxes"); and (3) volatiles (mostly H_2O and CO_2). Recent studies of melt and fluid inclusions trapped in pegmatite minerals provide new evidence for extreme enrichment of pegmatites in P, F and B (Webster et al. 1997; Peretyazko et al. 2000; Thomas et al. 2000). It appears that in some types of pegmatites, particularly the miarolitic and rare-element varieties, the abundances of non-silicate, fluxing components may reach levels of a few weight percent.

Despite the clear importance of fluxes for different aspects of pegmatite formation, flux-rich silicate systems need better experimental constraints. Previous experimental studies have examined individual effects of B, P and F on phase equilibria in granitic systems (Manning 1981; Pichavant 1987; London et al. 1993). However, in natural pegmatites several fluxing components are present together and their combined influence is likely to be more than merely the sum of individual effects. In this paper, we present the results of experiments using water-saturated synthetic peraluminous composition spiked with enough B_2O_3, P_2O_5 and F to simulate the most enriched compositions found in natural melt inclusions in pegmatite quartz (Thomas et al. 2000). The goal of our study was to examine the behaviour of fluxing components in hydrous aluminosilicate melts, i. e. factors which control their concentration levels and the effects of fluxes on phase equilibria and melt evolution. In view of the very enriched starting composition used in the experiments, our study is focused on the most evolved types of pegmatites and the latest stages of magma evolution.

Experimental and analytical methods

The synthetic starting mixture for the experiments was synthesised in the following way. A glass corresponding in composition to the dry eutectic of the $NaAlSi_3O_8$–$KAlSi_3O_8$–SiO_2 system was prepared from reagent-grade K_2CO_3, Na_2CO_3, Al_2O_3 and SiO_2. The compounds were mixed under acetone in an agate mortar, sintered in a Pt crucible until a constant weight was reached at 900 °C, then crushed and re-melted at 1,200 °C for 1 h. The glass was crushed again to fine powder and spiked with B_2O_3, P_2O_5 and F (5 wt% of each). Because the mixture was designed to model specific melt-inclusion compositions found in pegmatite quartz (Thomas et al. 2000), it was made strongly peraluminous by adding P and F in the form of aluminium-bearing chemicals ($AlPO_4$ and AlF_3). Boron was introduced in the form of boric acid (H_3BO_3). The rare alkalis Li, Rb and Cs were added as aqueous solutions of the hydroxides. The resulting, starting bulk composition is presented in Table 1. The mixture was dried at 300 °C and kept in a dessicator.

Table 1. Nominal composition of the starting mixture used in the experiments (*HP*) and the average composition of quartz-hosted melt inclusions of the Ehrenfriedersdorf pegmatite, Germany (Thomas, unpublished data). Both compositions are in wt%. *ASI* Alumina saturation index (mole ratio of Al_2O_3 to the sum of alkali oxides), *n.a.* not analysed

	HP	Ehrenfriedersdorf inclusions
SiO_2	59.30	62.0
Al_2O_3	17.91	11.7
B_2O_3	5.0	3.4
FeO	–	0.29
Na_2O	3.26	3.2
K_2O	4.14	3.0
Li_2O	0.5	n.a.
Rb_2O	1.0	0.61
Cs_2O	1.0	0.12
P_2O_5	5.0	3.2
F	5.0	4.49
Total	100	90.09
ASI	1.44	1.31

High-pressure experiments were carried out in cold-seal, rapid-quench pressure vessels using about 60 mg of the starting mixture and 15–20 mg H_2O in welded Pt and Au containers, 3 mm in diameter and 25 mm long. The runs were performed in the temperature range 450–900 °C and at pressures of 0.1 and 0.2 GPa. The amounts of water added to the charges provided vapour-saturated conditions. Equilibrium was checked by conventional methods of direct and reverse approaches (e.g. London 1992). For this purpose, some charges were first heated to 900 °C for about an hour, quenched and then annealed at lower temperatures. Run products synthesised from the original mixture and from homogeneous glass in pre-conditioned capsules showed no differences, and there was no indication of significant kinetic problems for crystallisation in our experiments.

Run products were mounted in epoxy resin and analysed for all the main components, except Li and B, by a Cameca SX-100 electron microprobe. Analyses were performed in WDS mode at 10-nA beam current and an accelerating voltage of 15 kV. Glasses were analysed with a defocused beam (beam size 20–40 μm). Almost all glasses were also analysed using a Cameca SX-50 microprobe equipped with the PC2 pseudo-crystal for light elements and a special analytical setup for quantitative B determination. B was analysed at 10 kV and 40 nA, using an anti-contamination cold trap cooled by liquid nitrogen. LaB_6 was taken as an internal standard, and synthetic glasses with B_2O_3 contents up to 20 wt% were used as external standards. Two methods were used: trace element mode (McGee et al. 1991) and peak area mode. A counting time of 300 s on the peak, a shift of +500 spectrometer steps, and the background from –5,200 to +8,000 steps were chosen for the trace-element mode. The peak area mode was run at 60 s, 10,000 steps, and 5 scans. The detection limit was 0.06 wt% of elemental B. Both methods yielded similar results within analytical uncertainty.

Results

Visual appearance of run products

At room temperature, products of the quench runs were composed of glass, crystalline solids and a drop of free aqueous solution. Some solids on capsule walls above the quenched glass beads undoubtedly precipitated from high-temperature hydrous fluids. Despite the high content of fluxes, the aluminosilicate melt readily quenched to a clear, transparent glass. After several weeks of storage, the glass became turbid and cracks developed at the surface, indicating loss of water. In most cases, minerals in the glass which crystallised from aluminosilicate melt are relatively large (dozens to hundreds of μm in length) and form well-shaped euhedral crystals. Surprisingly, mineral aggregates formed at near-solidus temperatures exhibit the same perfect shapes and large grain sizes as the dispersed crystals which grew at higher temperatures. At temperatures around 500–550 °C, there are still signs of gravitational separation of crystals and buoyant hydrous fluids. Thus, even at low temperatures the viscosity of aluminosilicate melt appears to be low. The same effect of low viscosity, enhanced crystal growth and gravitational settling was reported in a system doped with $Li_2B_4O_7$ (London 1986).

Crystallisation sequence

Crystallisation of the synthetic, water-saturated pegmatitic melt at 0.1 GPa (Table 2 and Fig. 1) starts

Table 2. Run conditions and mineral associations of run products. X_{H2O} Weight fraction of water in the charge. Abbreviations for the crystalline phases: *am* Amblygonite, *berl* berlinite, *cor* corundum, *cs* Cs-bearing aluminosilicate, *lac* lacroixite, *musc* muscovite, *qz* quartz, *tpz* topaz

Run No.	T (°C)	P (GPa)	Duration (day)	X_{H2O}	Crystal phases
HP-2	900	0.1	3	0.25	None
HP-5	800	0.1	5	0.25	Berl + tpz
HP-9	750[a]	0.1	20	0.25	Berl + tpz
HP-6	700	0.1	5	0.24	Berl + tpz + qz
HP-3	650	0.1	5	0.30	Berl + tpz + qz
HP-7	600	0.1	5	0.28	Berl + tpz + qz
HP-11	550[a]	0.1	14	0.26	Berl + musc + qz
HP-12	500[a]	0.1	14	0.24	Berl + musc + qz
HP-38	475[a]	0.1	7	0.15	Berl + musc + qz
HP-14	450[a]	0.1	21	0.24	Berl + musc + qz + am + lac + cs
HP-13	750[a]	0.2	7	0.25	Berl + tpz + traces cor
HP-16	700[a]	0.2	16	0.33	Berl + tpz + qz
HP-37	600[a]	0.2	7	0.14	Berl + musc + qz + tpz
HP-23	550[a]	0.2	4	0.25	Berl + musc + qz
HP-24	530[a]	0.2	4	0.26	Berl + musc + qz + am + lac
HP-15	500[a]	0.2	16	0.34	Berl + musc + qz + am + lac

[a]Before keeping charges at these temperatures for the specified duration of time, they were heated at 900 °C for 1 h and quenched

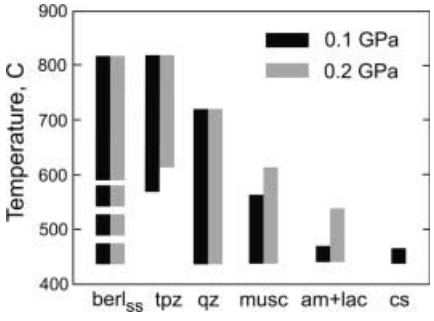

Fig. 1. Crystallisation sequence of the synthetic pegmatite composition. *Dashed lines* for berlinite denote temperature interval in which it is present only as exsolutions in berlinite-quartz composite crystals (see Table 2 for abbreviations of the mineral names)

between 800 and 850 °C with the appearance of berlinite ($AlPO_4$) and topaz. Quartz joins the mineral association between 700 and 750 °C. Topaz reacts with the melt and is replaced by muscovite between 550 and 600 °C. The association of mica, berlinite and quartz persists down to 475 °C. Just above the solidus, between 450 and 475 °C, a diverse range of minerals starts to crystallise and the proportion of residual melt decreases sharply. The near-solidus phases are Na and Li aluminophosphates (amblygonite and lacroixite) and a Cs-bearing aluminosilicate.

At 0.2 GPa the crystallisation sequence at temperatures higher than 600 °C is almost the same, the only difference being the appearance of a few corundum grains in run products at 750 °C. The increase in pressure appears to favour the stability of muscovite relative to topaz and shifts the onset of mica crystallisation up to about 620 °C. The stability of Na-Li aluminophosphates also shifts to higher temperatures; these phases start to crystallise between 530 and 550 °C. At 500 °C the proportion of crystalline solids is already very high and the system appears to be close to solidus. Thus, the solidus of the synthetic pegmatite is reached, depending on pressure, at temperatures between 450 and 500 °C. This is in a good agreement with solidus temperatures established for the natural Macusani peraluminous rhyolitic composition (London et al. 1988, 1989).

Crystalline phases

Berlinite and quartz

Berlinite and quartz are isostructural (Strunz 1941) and in our experiments these minerals form a series of intermediate solid solutions. The relationships between the phases and their mutual solubility appear to be strongly influenced by temperature. High-temperature liquidus berlinite forms small (5–15 μm) isometric grains with a composition close to that of the pure $AlPO_4$ end member (Table 3). At 700 °C, when quartz appears in the run products, berlinite and quartz crystallise as distinct separate phases. At this temperature quartz forms larger (10–30 μm) euhedral crystals which sometimes contain solid inclusions of berlinite (Fig. 2a, b). Microprobe studies reveal no significant SiO_2-$AlPO_4$ solid solution. By contrast, below 650 °C distinct berlinite grains are not observed, whereas mixed SiO_2-$AlPO_4$ crystals are predominant. Microprobe element dot maps reveal extensive zoning of the composite crystals with $AlPO_4$-rich cores and SiO_2-rich rims (Fig. 2c, d). This general pattern of the zoning is complicated by a "grainy" texture formed by small berlinite-rich specks, which often show regular crystallographic orientation and distribution within the composite crystals. We interpret these textures as due to exsolution of SiO_2-$AlPO_4$ homogenous crystals during quench. This interpretation is in agreement with the liquidus and subsolidus phase relationships on the SiO_2–$AlPO_4$ join (Horn and Hummel 1979).

Large, homogeneous euhedral crystals of quartz remain abundant in the run products down to the lowest, near-solidus temperatures (450–500 °C). According to

Table 3. Selected electron microprobe analyses of berlinite and quartz (wt%)

Phase	Berl	Berlinite–quartz-zoned crystals						Quartz	
Sample	HP-9	HP-6		HP-11		HP-37		HP-12	HP-38
T (°C)	750	700		550		600		500	475
P (GPa)	0.1	0.1		0.1		0.2		0.1	0.1
SiO_2	1.97	91.77	97.27	74.32	98.10	96.23	7.99	97.52	92.76
Al_2O_3	39.76	3.37	0.95	11.27	1.11	1.80	38.62	1.72	1.59
Na_2O	0.04	0.00	0.00	0.03	0.00	0.00	0.01	0.09	0.02
K_2O	0.13	0.01	0.00	0.03	0.02	0.02	0.01	0.29	0.03
P_2O_5	57.61	5.10	0.82	16.15	0.94	1.75	54.45	0.10	0.06
Total	99.50	100.25	99.04	101.80	100.16	99.81	101.08	99.72	94.46
Cations to 4 oxygens									
Si	0.04	1.83	1.97	1.47	1.96	1.93	0.16	1.96	1.97
Al	0.95	0.08	0.02	0.26	0.03	0.04	0.91	0.04	0.04
Na	0.00	0.00	0.00	0.00	0.00	0.00	0.00	0.00	0.00
K	0.00	0.00	0.00	0.00	0.00	0.00	0.00	0.01	0.00
P	0.99	0.09	0.01	0.27	0.02	0.03	0.92	0.00	0.00

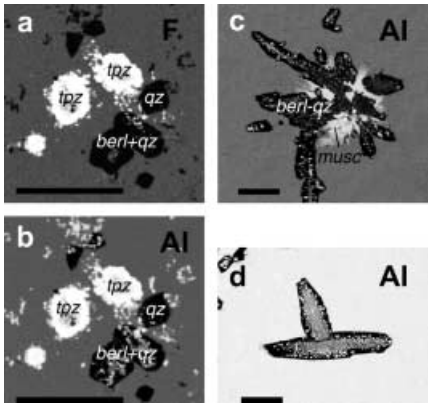

Fig. 2a–d. Electron microprobe dot maps of run products. **a, b** Images for F and Al in sample HP-6 (700 °C, 0.1 GPa) showing zoned topaz (*tpz*) aggregates and separate berlinite (*berl*) and quartz (*qz*) crystals in aluminosilicate glass. **c** A group of berlinite-quartz crystals and muscovite (*musc*) flakes suspended in aluminosilicate glass. Sample HP-11 (550 °C, 0.1 GPa). **d** Berlinite-quartz-zoned crystals in aluminosilicate glass, the same sample. *Scale bar* corresponds to 100 μm

microprobe analyses (Table 3), P_2O_5 contents are near or below the detection limits, but the crystals have measurable amounts of Al_2O_3, about 0.6–1.5 wt%. Low microprobe totals (in the range 95–99 wt%) indicate that undetected elements other than P, probably Li or H, charge-balance Al in the SiO_2 network. The virgilite substitution (LiAl = Si) is the most likely, because it was observed in similar circumstances in experiments with Macusani glass (London et al. 1989).

Topaz

Despite much interest in the magmatic stability limits of this mineral, very few experimental studies report liquidus topaz (e.g. Weidner and Martin 1987; Webster et al. 1987). In our study topaz is stable at temperatures above 550–600 °C. It forms small (3–7 μm) euhedral crystals scattered in the glass, but it is more commonly observed as large oval blebs which appear to be clusters or aggregates of small topaz crystals (Fig. 2a, b). Individual grains in these aggregates are visible only at the rims. The aggregates are chemically zoned, with Al/Si and F increasing from the core to the rim (Fig. 2a and Table 4). The rims of the aggregates as well as small, scattered crystals have compositions close to that of ideal topaz stoichiometry, whereas the cores have much lower Al/Si values and may be composed of some other Al-fluorosilicate. Both cores and rims contain high P_2O_5 concentrations which tend to increase with falling temperature, up to 6.4 wt% at 600 °C and 0.1 GPa.

Muscovite

Mica forms thin flakes which tend to group into spherical aggregates or to cluster in interstitial spaces between berlinite and quartz crystals (Fig. 2c). Typical analyses of muscovite are presented in Table 5. The compositions are fairly constant and show significant amounts of P_2O_5 and Rb_2O, which reflect the high bulk concentrations of these components in the starting composition and their relative compatibility with the muscovite structure. Low microprobe totals indicate that muscovite from our run products may also contain significant but undetected amounts of Li_2O and B_2O_3.

Li-Na aluminophosphates and minor accessory minerals

The high concentrations of P, F and B in our starting composition apparently prevented the crystallisation of feldspars (see discussion), which are the most abundant aluminosilicates in nature and major constituents of natural granitic pegmatites. In our experiments, the role of feldspars is partly taken by aluminophosphates, mostly lacroixite and amblygonite. Representative

Table 4. Compositions of topaz (see text for the discussion)

Sample	HP-6,		HP-3,		HP-7,	HP-13,	HP-16,	HP-37,
T (°C)	700		650		600	750	700	600
P (GPa)	0.1		0.1		0.1	0.2	0.2	0.2
Zone	Core	Rim	Core	Rim	Rim	Rim	Rim	Rim
SiO_2	57.47	31.42	57.57	30.07	24.24	29.44	28.23	25.10
Al_2O_3	34.28	54.40	33.04	54.36	56.64	55.96	56.94	56.94
Na_2O	0.03	0.07	0.01	0.04	0.07	0.00	0.00	0.07
K_2O	0.02	0.09	0.04	0.04	0.04	0.03	0.02	0.08
Rb_2O	0.04	0.08	0.07	0.01	0.01	0.01	0.01	0.04
Cs_2O	0.06	0.04	0.01	0.06	0.00	0.04	0.00	0.03
P_2O_5	3.00	3.51	3.23	5.14	6.44	1.61	2.94	5.34
F	11.58	18.25	11.11	18.33	19.01	18.91	19.05	20.87
Total	101.61	100.17	100.39	100.32	98.45	98.04	99.17	99.67
Cations to 4 oxygens								
Si	1.40	0.91	1.41	0.87	0.73	0.90	0.85	0.78
Al	0.99	1.87	0.96	1.86	2.02	2.01	2.01	2.08
P	0.06	0.09	0.07	0.13	0.16	0.04	0.07	0.14
F	0.90	1.68	0.86	1.68	1.82	1.82	1.81	2.04

Table 5. Compositions of muscovite (wt% and formula units)

Sample	HP-11	HP-12	HP-38	HP-14	HP-37	HP-23	HP-24
T (°C)	550	500	475	450	600	550	530
P (GPa)	0.1	0.1	0.1	0.1	0.2	0.2	0.2
n	9	5	3	4	4	3	5
SiO_2	45.12	45.77	49.80	45.48	46.81	49.04	46.93
Al_2O_3	36.00	35.87	36.86	35.32	35.02	36.94	34.57
Na_2O	0.48	0.38	0.28	0.31	0.60	0.35	0.40
K_2O	8.71	8.21	7.27	7.32	8.37	8.00	7.80
Rb_2O	1.14	1.18	0.80	1.27	1.51	1.07	1.21
Cs_2O	0.07	0.10	0.07	0.20	0.17	0.08	0.08
P_2O_5	1.25	1.80	0.73	1.53	1.45	0.85	0.86
F	3.29	3.03	2.70	2.46	3.33	2.83	2.66
Total	94.67	95.07	97.38	92.85	95.84	97.96	93.39
Cations to 11 oxygens							
Si	3.05	3.05	3.19	3.09	3.12	3.15	3.18
Al	2.86	2.82	2.79	2.83	2.75	2.80	2.76
Na	0.06	0.05	0.03	0.04	0.07	0.04	0.05
K	0.75	0.70	0.60	0.63	0.71	0.66	0.73
Rb	0.05	0.05	0.03	0.05	0.06	0.04	0.05
Cs	0.00	0.00	0.00	0.01	0.00	0.00	0.00
P	0.07	0.10	0.04	0.08	0.08	0.04	0.05
F	0.70	0.64	0.55	0.53	0.70	0.58	0.57

microprobe analyses of these phases are listed in Table 6. Both aluminophosphates have high F contents and are major hosts for this element at low temperatures.

During microprobe studies of the run products we also detected a few small grains of corundum (Table 2) with composition of almost pure Al_2O_3, and a Cs-bearing aluminosilicate. A microprobe analysis of the latter is presented in Table 6.

Aluminosilicate melt

Aluminosilicate melt is the most abundant fluid phase in our experiments down to temperatures of 500–550 °C. The chemical evolution of the melt is represented by glass compositions in the quenched run products listed in Table 7 and illustrated in variation diagrams in Fig. 3. At temperatures above 500 °C the concentrations of F, P and B in the glasses do not change significantly, indicating that the fluxes are effectively buffered by crystallisation of F- and P-rich minerals and by equilibria with immiscible fluids (discussed below).

The main feature of the chemical evolution of the melt is that crystallisation pushes it to silica-undersaturated compositions. This is best illustrated by projecting melt compositions onto the $NaAlSi_3O_8$ (Ab)–$KAlSi_3O_8$ (Or)–SiO_2 (Qz) ternary diagram (Fig. 4). In granitic systems, where feldspars are stable, the join $NaAlSi_3O_8$–$KAlSi_3O_8$ forms a thermal barrier and prevents liquid from evolving into the SiO_2-deficient region. This is not the case for our bulk composition. Peraluminosity and high F contents cause the substitution of orthoclase by muscovite,

Table 6. Compositions of amblygonite (*am*), lacroixite (*lac*) and Cs-bearing aluminosilicate (*cs*), wt% and formula units. *N* Number of analyses

Run No.	HP-14			HP-15		HP-24
T (°C)	450			500		530
P (GPa)	0.1			0.2		0.2
Phase	Lac	Am	Cs	Am	Am	Am
n	1	3	3	3	1	3
SiO_2	0.10	0.71	67.74	0.16	0.17	0.87
Al_2O_3	35.41	33.64	10.34	32.45	34.00	35.77
Na_2O	17.17	8.42	0.55	13.62	3.76	0.99
K_2O	0.00	0.12	1.97	0.01	0.02	0.17
Rb_2O	0.02	0.05	3.77	0.02	0.01	0.03
Cs_2O	0.08	0.02	9.27	0.02	0.05	0.01
P_2O_5	38.96	44.23	1.26	45.40	48.84	48.64
F	16.02	14.37	0.00	12.89	10.69	11.25
Total	101.01	95.51	94.92	99.14	93.04	92.98
Cations to 4 oxygens						
Si	0.00	0.02	1.68	0.00	0.00	0.02
Al	1.22	1.13	0.30	1.04	1.06	1.12
Na	0.97	0.47	0.03	0.72	0.19	0.05
K	0.00	0.00	0.06	0.00	0.00	0.01
Rb	0.00	0.00	0.06	0.00	0.00	0.00
Cs	0.00	0.00	0.10	0.00	0.00	0.00
P	0.97	1.07	0.03	1.05	1.10	1.09
F	1.48	1.30	0.00	1.11	0.90	0.94

Table 7. Compositions of glasses and hydrosaline globules (wt%). All values are averages of 4–7 individual microprobe analyses. *N.a.* Not analysed

Run No.	SiO_2	Al_2O_3	B_2O_3	Na_2O	K_2O	Rb_2O	Cs_2O	P_2O_5	F	Total
HP-2	59.90	16.59	1.7	2.82	3.71	1.14	0.99	4.28	4.00	93.44
HP-5	57.54	15.90	3.6	2.83	3.67	1.21	1.05	4.00	4.21	92.24
HP-9	60.79	14.92	1.8	2.98	3.84	1.11	1.02	3.25	3.81	91.92
HP-6	58.87	15.08	2.8	3.03	3.90	1.28	1.03	3.12	4.20	91.53
HP-3	57.37	15.84	2.6	3.08	4.10	1.40	1.23	3.32	4.03	91.27
HP-7	56.82	16.84	3.5	3.62	4.43	1.27	1.20	3.64	4.68	94.02
HP-11	53.34	18.14	4.2	3.89	4.35	1.46	1.50	3.88	5.23	93.79
HP-12	53.55	16.99	4.2	4.88	5.05	1.77	2.08	2.95	4.85	94.29
HP-38	50.73	17.08	n.a.	3.89	5.56	2.35	2.46	2.59	4.92	87.51
HP-14	16.53	11.29	n.a.	1.69	1.79	0.59	0.80	0.34	4.41	35.58
HP-13	56.60	15.69	3.8	2.62	3.64	1.24	0.99	3.58	4.44	90.74
HP-16	59.33	14.79	3.09	2.66	3.65	1.23	0.96	3.02	3.41	90.71
HP-37	53.71	16.92	5.2	3.39	4.40	1.50	1.30	3.42	4.77	92.60
HP-23	51.29	18.12	5.8	3.99	4.46	1.68	1.61	3.84	5.51	93.98
HP-23[a]	23.24	21.38	15.6	5.05	2.36	1.10	1.01	2.58	17.47	82.44
HP-24	52.20	17.39	5.9	2.92	4.21	1.78	1.96	3.86	3.88	92.46
HP-24[a]	20.23	19.71	8.7	3.12	1.96	0.73	0.77	2.68	15.26	66.73
HP-15	33.58	10.88	n. a.	0.35	0.93	1.22	4.86	0.12	0.46	52.20

[a]Hydrosaline globules

$$3KAlSi_3O_8 + 2Al_2O_3 + 2AlF_3 = 3KAl_3Si_3O_{10}F_2 \quad (1)$$
orthoclase melt muscovite

while high activities of P and F result in formation of Na-Li aluminophosphates and quartz instead of albite, for example,

$$2NaAlSi_3O_8 + P_2O_5 + 2F = 2NaAlPO_4F + 6SiO_2 \quad (2)$$
albite melt lacroixite quartz

Furthermore, strongly acid fluxes, such as F and P, increase the activity of SiO_2 (Manning 1981; London 1992) and extend the quartz field beyond the Ab-Or-Qz ternary. London et al. (1993) made a similar observation of liquid evolution across the feldspar barrier in the haplogranite system doped with P_2O_5.

Other fluids

Like more simple silicate-salt-H_2O systems, such as $NaAlSi_3O_8$–NaCl–H_2O and $NaAlSi_3O_8$–Na_2CO_3–H_2O (Koster van Groos and Wyllie 1966, 1969), our synthetic

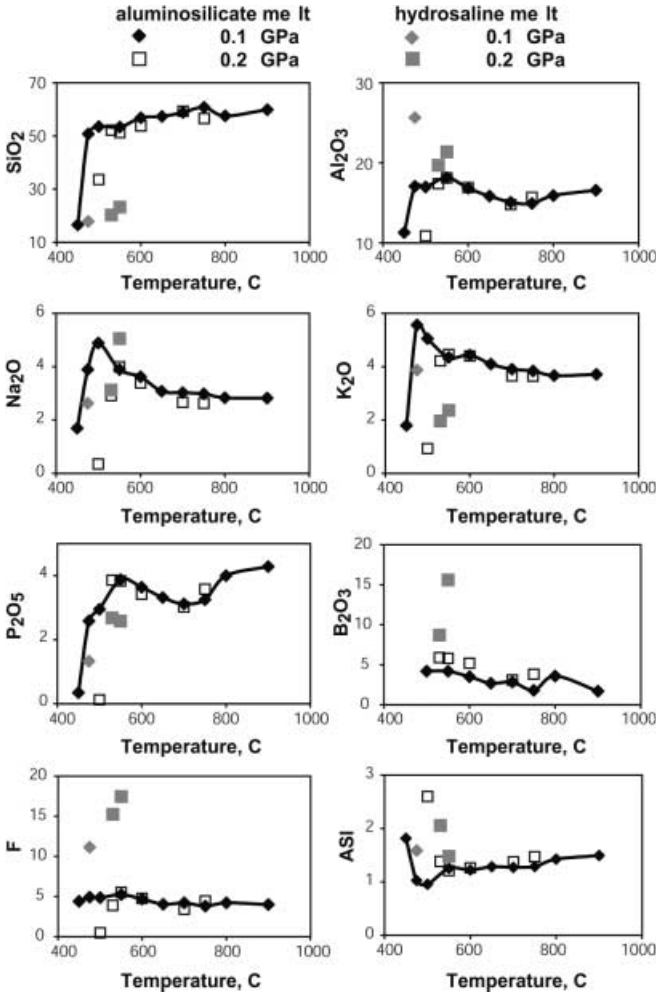

Fig. 3. Variation diagrams showing chemical evolution of aluminosilicate and hydrosaline melts at 0.1 and 0.2 GPa

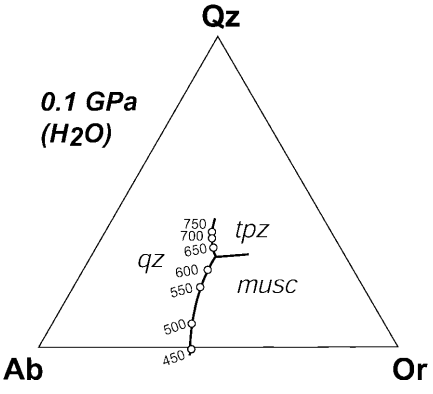

Fig. 4. Compositions of aluminosilicate glasses synthesised at 0.1 GPa projected on the albite (*Ab*) – orthoclase (*Or*) – quartz (*Qz*) ternary diagram. *Open circles* are experimental points, *numbers* indicate temperature. *Closed lines* are borders between topaz (*tpz*), quartz (*qz*), and muscovite (*musc*) crystallisation fields. Projection co-ordinates are calculated as follows: $Ab = Na_2O/0.118$; $Or = K_2O/0.169$; $Qz = SiO_2 – 0.687Ab – 0.648Or$, where Na_2O, K_2O and SiO_2 are bulk concentrations of the oxides in wt% in microprobe analyses (Table 7) and the coefficients equal to theoretical weight fractions of the oxides in Ab and Or

pegmatite system exhibits stable coexistence of aluminosilicate melt with two immiscible fluids of contrasting salinity: (1) concentrated hydrosaline melt (dense liquid, composed of molten salts with variable amounts of H_2O and silicate components), and (2) low-salinity hydrous fluid.

Recognising the presence of two hydrous fluid phases in quenched run products is not an easy task, especially at elevated, near-liquidus temperatures. The main problem is that both hydrosaline melt and dilute hydrous fluid do not quench to homogeneous solids, or to solid aggregates. Instead, during quench they condense to a loose mesh of crystals, tiny spherical shells of silicate glass, and a drop of liquid aqueous solution. The solids which precipitate from hydrous fluids in our experiments during quench are mostly crystals of H_3BO_3. The stable coexistence of two separate hydrous fluids was confirmed by in-situ experiments in a hydrothermal diamond cell, and by dynamic experiments in cold-seal pressure vessels (Veksler et al. 2002). In the static experiments and conventional quench runs considered here, hydrosaline melt was observed at subliquidus temperatures and high degrees of crystallisation. Under these conditions, hydrosaline melt is preserved as thin films and interstitial fillings covering the surfaces of crystals in aluminosilicate glass. It is especially common and abundant around radial aggregates of mica and, in such cases, large pools of hydrosaline melt (Fig. 5) can be polished and analysed by electron microprobe. However, determination of bulk composition is hampered by the extreme heterogeneity of such pockets, due to quench segregation of hydrosaline melt into at least two different glasses and a number of crystalline solids. Thus, only repeated broad-beam analyses and statistically representative averages give reasonable estimates of the bulk melt composition. Also, it is not always clear whether some portion of the neighbouring crystals may be quench phases of the melt and thus should be included into the bulk composition. Therefore, one should treat the analyses of hydrosaline melt listed in Table 7 as approximate.

Regardless of this uncertainty, microprobe results in Table 7 indicate the main components in the hydrosaline

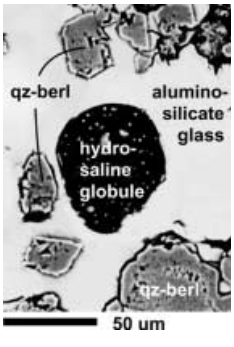

Fig. 5. Backscatter electron image of a globule of immiscible B- and F-rich liquid and aluminosilicate glass quenched at 550 °C and 0.2 GPa

melt and the general pattern of element partitioning between this phase and the aluminosilicate liquid. Mutual solubility of hydrosaline and aluminosilicate liquids at 530–550 °C and 0.2 GPa appears to be high. Hydrosaline melt contains 20–23 wt% SiO_2 and approximately the same amounts of Al_2O_3. Hydrosaline-aluminosilicate melt partition coefficients are significantly higher for Al than for Si (~1.2 vs. 0.4 by weight). Because of very high concentrations of F in hydrosaline melt (up to 17.5 wt%), a significant part of the Al is likely to form aluminofluoride species. The third major constituent of the hydrosaline melt is B_2O_3, which is probably in the form of hydrated species, like H_3BO_3 or alkali borates. Electron microprobe analyses show up to 16 wt% B_2O_3 in the quenched globules. As far as alkalis are concerned, Na partitions to the hydrosaline liquid, whereas K and heavier alkalis (Rb and Cs) are more compatible with the aluminosilicate melt. Hydrosaline-aluminosilicate melt partition coefficients for Na and K differ by more than a factor of 2 (1.3 vs. 0.53 by weight). This suggests the presence of a cryolite-like species (Na_3AlF_6) and is in agreement with previous studies of F-doped haplogranitic systems (Manning 1981; Gramenitskiy and Shchekina 1994).

The temperature and pressure effects on two-melt element partitioning are not clear because aluminosilicate and hydrosaline melts could only be distinguished and analysed with confidence in one sample from 0.1 GPa (HP-38) and two samples from 0.2 GPa (HP-23 and HP-24). At near-solidus temperatures both melt phases are preserved in small interstitial areas unsuitable for reliable analyses. Thus, analyses listed in Table 7 for samples HP-14 and HP-15 probably represent mixtures with quench products from both melts. Immiscible hydrosaline melt is sure to be present at higher temperatures as well, as indicated by the depletion of aluminosilicate glass in components which partition preferentially to hydrosaline liquid (B, F and Na). However, because of the lack of crystalline aggregates, serving as a trap, it is not preserved in run products. At higher temperatures, hydrosaline melt may also contain higher amounts of H_2O and this may also hamper its preservation. Pressure appears to have a stabilising effect on the hydrosaline liquid since its proportion relative to that of low-salinity fluid seems to be higher in samples synthesised at 0.2 GPa.

Little can be said about the composition of the low-salinity hydrous fluid, except that, judging by the appearance of its quench products, it contains significant amounts of H_3BO_3 and probably also water-soluble borates and alkali silicates.

Discussion

Our experimental study of a synthetic pegmatite composition reveals a number of complex mineral-melt reactions and fluid immiscibility phenomena. Many reactions observed in the system involve more than one of the fluxing components and are also linked to peraluminosity. The composition used in our experiments was oversaturated with B, P and F in order to establish their solubility limits in aluminosilicate melt and to reveal buffering reactions which may control the behaviour of these elements in natural pegmatites. In the following sections we explore some implications of our experimental results to natural pegmatitic systems, and discuss how our findings comply with existing models of pegmatite genesis.

Mineral-melt reactions and crystallisation control on solubility of fluxes

Miarolitic and rare-element pegmatites usually show unequivocal genetic links with granitic intrusions (Černý 1982), so a compositionally evolved granitic melt is an obvious starting point for pegmatite formation. At this early stage, concentrations of B, F and P as well as H_2O are likely to be moderate, but their incompatibility with major minerals (feldspars and quartz) should result in a continuous build-up in the melt during crystallisation until the appearance of minerals, or fluid phases with which the fluxes are compatible. In some cases and for some fluxes, "unlimited" accumulation may be possible, with gradual transformation of aluminosilicate melt to a fundamentally different, strongly fluxed fluid. Particular scenarios for B, P and F were discussed by London (1987, 1992, 1997). Here, we consider new constraints on phase equilibria of these components, which were revealed in our study.

Phosphorus

Our synthetic pegmatite is probably the first experimental example of a geologically relevant system in which the solubility of P in the melt is controlled by crystallisation of berlinite ($AlPO_4$). This is a consequence of high P_2O_5 contents and strong peraluminosity of the bulk composition, as well as the nominal absence of CaO and consequent lack of common Ca phosphates such as apatite. Berlinite is the first liquidus phase, and significant amounts of the $AlPO_4$ component are also present in other minerals crystallising in the system. At low temperatures, Na-Li aluminophosphates provide the main sink for P. In contrast to metaluminous compositions (London et al. 1993), the berlinite control on P solubility prevents extreme P enrichment in residual aluminosilicate melts. Above 500 °C the P_2O_5 contents in the aluminosilicate melt stay within the limits of 2.6–4.0 wt% (Table 7 and Fig. 3). Among the three immiscible fluids in the synthetic pegmatite, aluminosilicate melt has the highest P_2O_5 content and low-salinity hydrous fluid is likely to have the lowest.

London et al. (1993) showed that feldspars are important hosts for P in peraluminous granitic systems, but these phases are not stable in our experiments.

According to Eq. (2) above, the combined effect of peraluminosity and high activities of P and F results in stability of Li-Na aluminophosphates instead of albite. The same reaction was documented in a recent experimental study of amblygonite-montebrasite liquidus equilibria (London et al. 2001). It was shown that at low concentrations of F liquidus montebrasite coexisted with alkali feldspar whereas, at higher F and in equilibrium with amblygonite end member, feldspar became unstable.

Fluorine

In the fluids and minerals synthesised in our experiments F, like P, is clearly associated with Al. At near-liquidus temperatures the solubility of F in aluminosilicate melt is limited by topaz crystallisation and the separation of hydrosaline fluid. As temperature decreases, the buffering role is taken over by muscovite and F-rich Li-Na aluminophosphates. The concentrations of F in aluminosilicate melt during crystallisation vary from 3.4 to 5.5 wt% (Table 7). According to the semiquantitative analyses, F contents in the coexisting hydrosaline melt appear to be at least three times higher.

The instability of K-feldspars in our experiments is definitely a consequence of F oversaturation of the starting bulk composition. The formation of muscovite at the expense of orthoclase (Eq. 1) is a typical feature of evolution in peraluminous pegmatites (Fenn 1986; London et al. 1988, 1989; London 1992).

Boron

Within the studied temperature interval, B is the only major component of the synthetic pegmatite composition which remains incompatible with any liquidus mineral. In view of the strong peraluminosity and high bulk Li_2O content, tourmaline (e.g. elbaite) was expected to crystallise in the run products. This, however, is not the case and in the absence of tourmaline and other B minerals, B concentrations in the aluminosilicate melt are buffered by partitioning to hydrosaline melt and, to a lesser degree, to low-salinity fluid. The reason for tourmaline instability is not clear, but our experiments suggest that high F, or P activities may affect tourmaline stability and determine the behaviour of B in natural pegmatites.

Conditions for formation of immiscible boro-aluminofluoride melt

Hydrosaline melt coexists with aluminosilicate melt and lower-salinity aqueous fluid over a broad range of P-T conditions in our experiments. Fluid immiscibility requires a fundamental difference in the nature of chemical bonding in coexisting phases. In our synthetic pegmatite, as in other silicate-salt-H_2O systems, aluminosilicate melts have predominantly covalent bonds and are characterised by a strong tendency for polymerisation whereas hydrosaline melts, with predominantly ionic bonds, and low-density hydrous fluids, loosely bound by weak inter-molecular forces, are totally depolymerised.

Hydrosaline melt in our experiments is composed mainly of aluminofluoride and hydrated borate species. Thus, peraluminosity, high bulk B_2O_3/H_2O and F contents appear to be the main factors favouring this type of liquid immiscibility. As mentioned above, increase in pressure from 0.1 to 0.2 GPa appeared to stabilise the denser hydrosaline melt relative to low-salinity fluid. The importance of peraluminosity is supported by recent experimental results by Sowerby and Keppler (2002), who observed complete miscibility between aluminosilicate melt and hydrous fluid and supercritical behaviour at 0.5 GPa and 595 °C in experiments with peralkaline B- and F-rich synthetic pegmatite. Thus, the position of the critical curve in P-T space appears to be strongly dependent on the bulk alkali-alumina ratio. With regard to the concentration of fluxes, it is important to note that immiscibility occurs at quite moderate concentrations of B_2O_3, F and P_2O_5 (~3.5–4.5 wt% of each) on the aluminosilicate side of the solvus. Such concentrations of fluxing components are realistic at least for some types of natural pegmatites (London 1992), and similar concentrations of B_2O_3 and F were reported for residual aluminosilicate melt at 650 °C and 0.2 GPa in experiments with Macusani glass without added water (London et al. 1989). The important conclusion is that levels of B and F enrichment which are needed to form immiscible boro-alumofluoride hydrosaline melt can be reached during crystallisation of natural pegmatites and such melts should be present in nature. In experimental products, hydrosaline melt is hard to detect, especially if present in small quantities, and we believe that it has been overlooked in some previous experiments.

Implications of hydrosaline melt for features of natural pegmatites

Traces of high-salinity fluid rich in B and aluminofluoride species have been documented in numerous studies of fluid inclusions in pegmatite quartz (e.g. Roedder 1992; Peretyazko et al. 2000; Thomas et al. 2000), and until now the idea of multiple pegmatitic fluids and fluid immiscibility as a factor for internal differentiation of pegmatite bodies has been more popular among researchers of melt and fluid inclusions than among experimental petrologists. The experimental demonstration of three immiscible fluid phases is an important addition to the classical concepts of pegmatite development, and it provides a crucial confirmation of fluid and melt-inclusion studies. More experiments are needed for full characterisation of hydrosaline pegmatitic melt, but our new findings encourage examination of some of the much-debated features of granitic pegmatites from a new perspective.

Viscosity, density, wetting properties and melt percolation

The low viscosity of aluminosilicate and hydrosaline melts combined with significant density difference between them and the low-salinity fluid result in effective gravitational separation of these phases in our experiments. Efficient separation should also take place in nature wherever such type of liquid immiscibility occurs. The tendency of hydrosaline melt to wet surfaces of silicate minerals should make it highly mobile at the final stages of crystallisation, and this may explain why hydrosaline inclusions are so abundant in pegmatite minerals. In view of its mobility, hydrosaline melt should also be a very effective agent of chemical transport, and it may account for the extensive mineral reactions typical of low-temperature zones in miarolitic and rare-element pegmatites.

Mineralogical and chemical zonation of pegmatite bodies

Hallmarks of many pegmatites are spectacular local variations in the sizes and proportion of main rock-forming minerals, and extensive chemical zoning. Although each pegmatitic body is unique, common general patterns of the zonation have been established, as described in a number of reviews (e.g. Černý 1982). Many of these features, especially at a scale of individual crystals, may result from disequilibrium crystallisation and boundary-layer effects (London et al. 1989; London 1992, 1999). However, at a larger scale relevant to whole pegmatite bodies, fluid immiscibility and the spatial separation of phases provide a much more effective means of chemical differentiation. In view of the unusual physical properties of flux-rich pegmatitic fluids, convection and gravitational phase separation should not be dismissed (e.g. London 1999).

One of the common patterns of large-scale zonation is demonstrated by complex relationships between feldspars. Plagioclase-rich outermost zones gradually change to intermediate graphic and blocky zones dominated by K-feldspar, but in the most evolved central zones and replacement bodies feldspars are represented by almost pure albite varying in texture from banded, saccharoidal units to coarse-grained clevelandite (Černý 1982; London 1992). Finally, the quartz cores are essentially feldspar-free. Liquid immiscibility between aluminosilicate and F-rich hydrosaline melts may explain the observed strong fractionation of Na from K. Higher affinity of Na (and Li) to aluminofluoride species was demonstrated earlier in an F-doped haplogranitic system (Glyuk and Shinakin 1986; Gramenitskiy and Shchekina 1994), where it was shown that Na partitions strongly to the immiscible cryolitic liquid and the addition of F decreased the albite crystallisation field much more than that of K-feldspar (Manning 1981). As a result, Na may be transported by hydrosaline melt more effectively than K, and the stability limits of albite and K-feldspar are different.

Our experiments may explain some important details of greisenisation, which takes place in the central zones of pegmatites. Quartz and muscovite remain stable in equilibrium with hydrosaline melt with only 20 wt% SiO_2 whereas feldspars are totally absent. It is also important that albite and K-feldspar are involved in different reactions (Eqs. 1 and 2) and their stabilities depend on different fluxes. Phase equilibria in our experiments do not provide direct evidence of albite and K-feldspar stability, because in this particular composition both feldspars are unstable. However, Gramenitskiy and Shchekina (1994) demonstrated that in an F-spiked granitic system feldspars do crystallise in equilibrium with an immiscible aluminofluoride melt, and it is reasonable to suggest that, if the P_2O_5 content of the bulk composition used in our runs is decreased, Na could not be totally incorporated into aluminophosphates and some late-stage albite will form. Further experiments are underway to confirm these relationships.

Sharp contacts, asymmetric textures and enhanced crystal growth

In discussing the spectacular and enigmatic textural relationships between late-stage albitic aplite and massive quartz in Tanco pegmatite (Manitoba), London (1992) pointed out that sharp contacts and curved shapes of aplite bodies resemble interfaces between two immiscible fluids. In light of new experimental evidence presented here, this resemblance may indeed reflect the percolation of aluminosilicate and hydrosaline melts, both of which should carry significant proportions of crystals, at such a late stage of pegmatite evolution. Because of the apparently large contrast in physical properties (density, viscosity, wetting angles, etc.), the interface between hydrosaline liquid and aluminosilicate melt should be sharp. As to the crystal content, although in theory both immiscible liquids are in equilibrium with the same mineral assemblage, hydrosaline melt and its aluminosilicate counterpart should provide quite different conditions for crystal growth. As a result, some minerals may preferentially crystallise from one or the other melt. Textures of the resulting crystal aggregates should be also quite different. Hydrosaline liquid, being similar to technological fluxes used in industrial crystal growth, should provide much better conditions for formation of gigantic, perfectly shaped individual crystals. This media meets the criteria imposed by Roedder (1992) for the source of gem-quality crystals in miarolitic zones, because the residual hydrosaline melt will form water-soluble masses which can be removed by post-magmatic hydrothermal leaching. Finally, gravitational segregation of the immiscible melts may be one reason for the common observation of asymmetric textures and zonation pattern, where larger and better formed crystals occur at the hanging wall or roof of pegmatite bodies.

Formation of rare-element ores

In comparison to the low-salinity aqueous fluid, hydrosaline and aluminosilicate melts are likely to be much more effective agents of transport and accumulation of economically important trace elements. The exact role of these fluids in the formation of rare-element ores in pegmatites will become clear only after better constraints on trace-element partitioning between the immiscible phases. Effects of liquid immiscibility on some elements have been studied (e.g. Gramenitskiy et al. 1995; Zhu et al. 1996). Full and accurate quantification of the trace-element partitioning is a challenging task for future experiments, because analysing hydrosaline melt and separating it from low-density aqueous fluid is anything but easy. Potentially, however, this type of liquid immiscibility may hold a clue to many poorly understood chemical and mineralogical features of diverse rare-element ores related to granitic pegmatites.

Acknowledgements We thank Dr. Dieter Rhede and Oona Appelt for the help with microprobe analyses. We are grateful to Drs. Wilhelm Heinrich and Robert Trumbull for fruitful discussions and much help in preparation of this paper. We appreciate constructive and helpful reviews provided by Drs. Andreas Audetat and John Sowerby. This study was supported by a grant of the Deutsche Forschungsgemeinschaft priority program "Formation, transport and differentiation of silicate melts" to R.T. (TH 489/2-1).

References

Bodnar RJ, Burnham CW, Sterner SM (1985) Synthetic fluid inclusions in natural quartz. III. Determination of phase equilibrium properties in the system H_2O–NaCl to 1000 °C and 1500 bars. Geochim Cosmochim Acta 49:1861–1873

Černý P (1982) Anatomy and classification of granitic pegmatites. In: Černý P (ed) Short course in granitic pegmatites in science and industry. Mineralogical Association of Canada, Winnipeg, pp 1–39

Fenn PM (1986) On the origin of graphic granite. Am Mineral 71:325–330

Glyuk DS, Shinakin BM (1986) The role of liquid-immiscibility differentiation in the pegmatite process. Geochem Int 23(8):38–49

Gramenitskiy YeN, Schekina TI (1994) Phase relationships in the liquidus part of a granitic system containing fluorine. Geochem Int 31(1):52–70

Gramenitskiy YeN, Schekina TI, Romanenko IM (1995) The nature of tungsten specialization of granites in the light of experimental data (in Russian). Doklady Akad Nauk 340:801–804

Horn WF, Hummel FA (1979) The system $AlPO_4$ – SiO_2. Glass Ceram Res Bull 26:47–59

Jahns RH, Burnham CW (1969) Experimental studies of pegmatite genesis. I. A model for the derivation and crystallization of granitic pegmatites. Econ Geol 64:843–864

Koster van Groos AF, Wyllie PJ (1966) Liquid immiscibility in the system Na_2O-Al_2O_3-SiO_2-CO_2 at pressures up to 1 kilobar. Am J Sci 264:234–255

Koster van Groos AF, Wyllie PJ (1969) Melting relationships in the system $NaAlSi_3O_8$–NaCl–H_2O at one kilobar pressure, with petrological applications. J Geol 77:581–605

London D (1986) Magmatic-hydrothermal transition in the Tanco rare-element pegmatite: evidence from fluid inclusions and phase equilibrium experiments. Am Mineral 71:376–395

London D (1987) Internal differentiation of rare-element pegmatites: effects of boron, phosphorus and fluorine. Geochim Cosmochim Acta 51:403–420

London D (1992) The application of experimental petrology to the genesis and crystallization of granitic pegmatites. Can Mineral 30:499–540

London D (1997) Estimating abundances of volatile and other mobile components in evolved silicic melts through mineral-melt equilibria. J Petrol 38:1691–1706

London D (1999) Melt boundary layers and the growth of pegmatite textures. Can Mineral 37:826–827

London D, Hervig RL, Morgan GB IV (1988) Melt-vapor solubilities and element partitioning in peraluminous granite-pegmatite systems: experimental results with Macusani glass at 200 MPa, and the internal differentiation of granitic pegmatites. Contrib Mineral Petrol 99:360–373

London D, Morgan GB IV, Hervig RL (1989) Vapor-undersaturated experiments with Macusani glass + H_2O at 200 MPa, and the internal differentiation of granitic pegmatites. Contrib Mineral Petrol 102:1–17

London D, Morgan GB IV, Babb HA, Loomis JL (1993) Behavior and effects of phosphorus in the system Na_2O-K_2O-Al_2O_3-SiO_2-P_2O_5-H_2O at 200 MPa(H_2O). Contrib Mineral Petrol 113:450–465

London D, Morgan GB IV, Wolf MB (2001) Amblygonite–montebrasite solid solutions as monitors of fluorine in evolved granitic and pegmatitic melts. Am Mineral 86:225–233

Manning DAC (1981) The effect of fluorine on liquidus phase relationships in the system Qz-Ab-Or with excess water at 1 kb. Contrib Mineral Petrol 76:206–215

McGee JJ, Slack JF, Herrington JR (1991) Boron analysis by electron microprobe using MoB_4C layered synthetic crystals. Am Mineral 76:681–684

Peretyazhko IS, Prokof'ev VYu, Zagorskii VE, Smirnov SZ (2000) Role of boric acids in the formation of pegmatite and hydrothermal minerals: petrologic consequences of sassolite (H_3BO_3) discovery in fluid inclusions. Petrology 8:214–237

Pichavant M (1987) Effects of B and H_2O on liquidus phase equilibria in the haplogranite system at 1 kbar. Am Mineral 72:1056–1070

Roedder E (1992) Fluid inclusion evidence for immiscibility in magmatic differentiation. Geochim Cosmochim Acta 56:5–20

Shmulovich KI, Churakov SV (1998) Natural fluid phases at high temperatures and low pressures. J Geochem Explor 62:183–191

Sourirajan S Kennedy GC (1962) The system H_2O-NaCl at elevated temperatures and pressures. Am J Sci 260:115–141

Sowerby JR, Keppler H (2002) The effect of fluorine, boron and excess sodium on the critical curve in the albite-H_2O system. Contrib Mineral Petrol 143:32–37

Strunz H (1941) Isotypie von Berlinit mit Quartz. Z Kristallogr 103:228–229

Thomas R, Webster JD, Heinrich W (2000) Melt inclusions in pegmatite quartz: complete miscibility between silicate melts and hydrous fluids at low pressure. Contrib Mineral Petrol 139:394–401

Veksler IV, Thomas R, Schmidt C (2002) Experimental evidence of three coexisting immiscible fluids in synthetic granite pegmatite. Am Mineral 87:775–779

Webster JD, Holloway JR, Hervig RL (1987) Phase equilibria of a Be, U and F-enriched vitrophyre from Spor Mountain, Utah. Geochim Cosmochim Acta 51:389–402

Webster JD, Thomas R, Rhede D, Förster H-J, Seltmann R (1997) Melt inclusions in quartz from an evolved peraluminous pegmatite: geochemical evidence for strong tin enrichment in fluorine-rich and phosphorus-rich residual liquids. Geochim Cosmochim Acta 61:2589–2604

Weidner JR, Martin RF (1987) Phase equilibria of the fluorine-rich leucogranite from the St. Austell pluton, Cornwall. Geochim Cosmochim Acta 51:1591–1597

Zhu Y, Zeng Y, Ai Y (1996) Experimental evidence for a relationship between liquid immiscibility and ore-formation in felsic magmas. Applied Geochem 11:481–487